Hadronic and electromagnetic fragmentation of ultrarelativistic heavy ions at LHC

H. H. Braun,[1] A. Fassò,[2] A. Ferrari,[3] J. M. Jowett,[3] P. R. Sala,[4] and G. I. Smirnov[3,5,*]

[1]*Paul Scherrer Institut, 5232 Villigen PSI, Switzerland*
[2]*ELI Beamlines, Prague, Czech Republic*
[3]*CERN, CH-1211 Geneva, Switzerland*
[4]*INFN, Via Celoria 16, 20133 Milano, Italy*
[5]*Laboratory for High Energy Physics, JINR, Dubna, Russia*

(Received 8 July 2013; published 24 February 2014)

Reliable predictions of yields of nuclear fragments produced in electromagnetic dissociation and hadronic fragmentation of ion beams are of great practical importance in analyzing beam losses and interactions with the beam environment at the Large Hadron Collider (LHC) at CERN as well as for estimating radiation effects of galactic cosmic rays on the spacecraft crew and electronic equipment. The model for predicting the fragmentation of relativistic heavy ions is briefly described, and then applied to problems of relevance for LHC. The results are based on the FLUKA code, which includes electromagnetic dissociation physics and DPMJET-III as hadronic event generator. We consider the interaction of fully stripped lead ions with nuclei in the energy range from about one hundred MeV to ultrarelativistic energies. The yields of fragments close in the mass and charge to initial ions are calculated. The approach under discussion provides a good overall description of Pb fragmentation data at 30 and 158*A* GeV as well as recent LHC data for $\sqrt{s_{\mathrm{NN}}} = 2.76$ TeV Pb-Pb interactions. Good agreement with the calculations in the framework of different models is found. This justifies application of the developed simulation technique both at the LHC injection energy of 177*A* GeV and at its collision energies of 1.38, 1.58, and 2.75*A* TeV, and gives confidence in the results obtained.

DOI: 10.1103/PhysRevSTAB.17.021006 PACS numbers: 25.70.De, 25.70.Mn, 25.70.Kk, 25.75.-q

I. INTRODUCTION

The passage of fast heavy ions through a medium involves various phenomena which strongly depend on the energy and charge states of the incident ions. The latest experimental and theoretical achievements in this field of research became subjects of recent reviews [1,2]. Generally, the phenomena under discussion can be classified into three broad categories: (1) inelastic collisions of ions with target nuclei, (2) inelastic collisions of ions with target electrons, and (3) elastic ion collisions with target atoms.

The advent of the LHC [3], which will eventually produce lead-lead collisions with the energy of 2750*A* GeV for each beam, poses many novel challenges to accelerator beam theory. In particular, the interaction of the most energetic ion beams available on Earth with various materials needs to be considered and quantitatively described. In contrast to the proton-proton mode of LHC operation, the fragmentation of projectile ions must be considered in detail. The beam loss and collimation efficiency estimates at the LHC depend directly on predictions of the yields of fragments close in mass and charge to the initial ions [4–6]. The distribution of magnetic rigidity (about 1%) of the fragments results in their being selectively lost in different places within the collimation insertions. Sufficiently concentrated energy deposition can lead to magnet quenching and the interruption of collider operation. It is therefore important to understand the loss patterns and study means to mitigate the likelihood of quenches.

The present paper is focused on those interactions of fully stripped ultrarelativistic ions which belong to category (1) above. Inelastic interaction of projectiles with target nuclei involving hadronic and electromagnetic forces is considered. The latter become dominant in the ultraperipheral collisions leading to the electromagnetic dissociation (EMD) of nuclei. This reaction channel is under intense study in relation to experiments at the Relativistic Heavy Ion Collider (RHIC) and Large Hadron Collider (LHC) [7–12]. We do not discuss in this paper the stopping and energy loss of ultrarelativistic ions in matter but rather concentrate on fragmentation reactions with the aim of describing the yields of fragments close in mass and charge to the projectile nuclei. The contribution from the reactions which fall into categories (2) and (3) can be considered as a small correction to the outcome of the reactions of category (1); it is briefly commented on below. Our results can be directly compared

*george.smirnov@cern.ch

to experimental data obtained in heavy-ion fragmentation studies on thin targets. Following these tests, the results on fragment yields and models can in turn be used in macroscopic transport calculations.

The contributions of such processes and characteristics of produced fragments are studied within the framework of the FLUKA code [13,14]. A brief description of the approach is given in Secs. II and III where relevant physical processes are also discussed. In Sec. IV the validity of the method is verified by comparison with the fragmentation data obtained at CERN Super Proton Synchrotron (SPS) [15–19]. In Sec. V we present results of calculations of beam fragmentation at the LHC collider at injection energy of 177A GeV and at the energy of the SPS circulating beam of 106.4A GeV used for machine development experiments [20]. We also present results at collision energy of 1.38A TeV corresponding to Pb-Pb interactions at $\sqrt{s_{\mathrm{NN}}} =$ 2.76 TeV per colliding nucleon pair and compare them with recent LHC data reported by the ALICE Collaboration [21,22]. In addition, the results that we obtained at beam energies of 1.58 and 2.75A TeV can serve as predictions for new measurements at the LHC collider.

II. HADRONIC INTERACTIONS IN FLUKA/DPMJET-III

The range of impact parameter, b, in hadronic interactions of nuclei extends from complete overlap of nuclei in central collisions, $b \simeq 0$, up to grazing interactions in peripheral collisions, $b \simeq R_1 + R_2$. Here R_1 and R_2 denote the nuclear radii. The two-component dual parton model implemented in the DPMJET-III code is used to describe production of nuclear fragments in ion-ion hadronic collisions. DPMJET-III provides a general approach to describe hadron-hadron, hadron-nucleus and nucleus-nucleus collisions at accelerator and cosmic ray energies.

FLUKA [13,14] is a transport and interaction Monte Carlo code, capable of handling hadronic and electromagnetic showers from thermal neutrons up to the LHC design energy of 14 TeV. FLUKA hadronic interaction models are based, as far as possible, on well tested microscopic models. The models ensure a high level of accuracy and versatility, they preserve correlations within interactions and among the shower components, and they provide predictions where no experimental data is directly available. The hadron-nucleus nuclear interaction model of FLUKA, called PEANUT, is a four step model. At high energies the Gribov-Glauber multiple collision formalism is implemented, and particle production is simulated within the framework of the dual parton model. Secondaries are then followed through the nucleus taking into account the formation zone concept, allowing for reinteractions within the framework of a generalized intranuclear cascade approach. After energetic particles are emitted or reinteract up to the point where all remaining nucleons have energies below a few tens of MeV, an exciton based preequilibrium model is applied until the system is fully thermalized. The residual excitation is then spent in the emission of evaporation particles and deexcitation photons. Depending on the initial projectile energy some of the previous stages can be omitted. For example, for incident energies below 30–50 MeV only the preequilibrium and evaporation stages are performed. A detailed description of the PEANUT model and extensive benchmarking can be found in the literature [23–28]. The most recent developments of the PEANUT event generator are described in Refs. [25–29]. The evaporation, fission and fragmentation models, while still based on the approaches described in Refs. [23,30,31], have undergone significant improvements along the years, some of them are of particular relevance for this work: details can be found in Refs. [24,26,28,29]. A further development in the evaporation model has been worked out specifically for this paper. Spin and parity effects are now accounted for at low excitations resulting from photon interactions along the lines of what has been already implemented for light nuclei and described in [28,29]. The minimum angular momentum, L_{min}, required for the emission of particles from configurations of known spin and parity and populating the allowed levels J^{π} is computed. If the neutron emission is forbidden with $L = 0$, a suitable centrifugal barrier is computed and added to the reaction Q-value resulting in a lower emission probability. As a practical example of relevance for this paper, photon interactions on ^{208}Pb in the giant dipole resonance (GDR) region would result in a compound nucleus with angular momentum $J^{\pi} = 1^{-}$. After the emission of a neutron with $L = 0$, the excited ^{207}Pb remnant can be either $J^{\pi} = \frac{3}{2}^{-}$ or $J^{\pi} = \frac{1}{2}^{-}$. In both cases a further neutron emission with $L = 0$ can only end up on relatively high-lying states of ^{206}Pb since most low-lying states have positive parity and, therefore, are incompatible with the emission with $L = 0$ from a negative-parity state.

In order to extend FLUKA to nucleus-nucleus collisions, the DPMJET-III [32,33] code has been interfaced to cover the high ($> 5A$ GeV) energy range, and an extensively modified version of the RQMD-2.4 code [34,35] is used at lower energies. DPMJET-III is a Monte Carlo model for sampling hadron-hadron, hadron-nucleus and nucleus-nucleus collisions at accelerator and cosmic ray energies (E_{lab} from 5–10A GeV up to 10^9–$10^{11}A$ GeV). It is implemented in FLUKA as an event generator to simulate nucleus-nucleus interactions exclusively. DPMJET-III, as well as the FLUKA high energy hadron-nucleus generator, is based on the dual parton model in connection with the Glauber formalism.

DPMJET-III manages the fast stage of nuclear collisions: the code computes the mass, charge, and excitation of the residual prefragment nucleus. The following deexcitation and evaporation of the excited residual nuclei, and the generation of the final fragments, are performed by calling the FLUKA evaporation, fission, and fragmentation modules [23,24,30], including the developments and improvements described

above. A description of this procedure applied to the predecessor of the DPMJET-III code can be found in [30,31].

III. ELECTROMAGNETIC DISSOCIATION OF HEAVY IONS

A. Electromagnetic dissociation of relativistic heavy ions

One or both colliding nuclei can breakup in the high-intensity electromagnetic fields involved in ultraperipheral collisions without direct overlap of nuclear densities, at $b > R_1 + R_2$. At relativistic energies the Lorentz-contracted Coulomb fields of colliding nuclei can be represented as swarms of virtual photons, as suggested by the Weizsäcker-Williams method [36]. Absorption of equivalent photons by a nucleus leads to its excitation followed by various de-excitation processes via emission of neutrons, protons, mesons and even light nuclear fragments. Such photonuclear reactions are given the collective name electromagnetic dissociation of nuclei. The majority of theoretical work in studies of the electromagnetic dissociation has been done in the framework of the Weizsäcker-Williams approximation (WWA), see e.g., [7,8,37]. The uncertainty of the approximation is discussed in a recent review [9] and is considered as satisfactory with regard to the present status of its experimental verification. Our interest in EMD processes is dictated by the fact that in the LHC ion beam nuclear remnants close in mass and charge to initial ions are mostly created by electromagnetic dissociation of heavy lead nuclei. Moreover, an appreciable number of light fragments with a momentum-to-charge ratio close to that of the main circulating beam are also produced in EMD.

The FLUKA model employs its internal nuclear interaction generator, PEANUT, in order to describe photonuclear reactions induced by both real and virtual photons. The model is described in Refs. [28,38,39]. Electromagnetic dissociation has been implemented in this framework. This involves an equivalent photon spectrum $n(\omega)$ and the cross sections for the (quasireal) photon-nuclear reactions $\sigma_\gamma(\omega)$, where ω is the virtual photon energy. The latter cross sections are considered to be induced by the single (equivalent) photon absorption process:

$$\gamma + A \to A' + X. \tag{1}$$

The standard approach developed for the evaluation of the one-photon cross section σ_{EMD} involves consideration of the *equivalent photon spectrum* $n(\omega)$ corresponding to the projectile nuclei. The target nucleus is considered to be at rest. According to the concept of equivalent photons, the cross section factorizes into $n(\omega)$ and the cross section for the γA interaction $\sigma_\gamma(\omega)$:

$$\sigma_{\mathrm{EMD}} = \int_{\omega_{\min}}^{\omega_{\max}} \frac{d\omega}{\omega} n(\omega)\sigma_\gamma(\omega), \tag{2}$$

where the integration limits are determined as follows:

$$\omega_{\min} = E_{\mathrm{thr}}, \tag{3}$$

and

$$\omega_{\max} \approx \frac{\gamma}{R_A}, \tag{4}$$

where E_{thr} is the threshold energy of the single nucleon emission due to the EMD reaction, R_A is the charge radius of the projectile nucleus which is approximated as $1.2 \cdot A^{1/3}$ fm, and γ is the relativistic Lorentz factor.

The equivalent photon spectrum in the leading logarithmic approximation is given by [8]

$$n(\omega) = \frac{2Z^2\alpha}{\pi} \ln\left(\frac{\gamma}{\omega R_A}\right). \tag{5}$$

Here α is the fine structure constant and Z is the atomic number of the projectile nucleus.

The physics underlying processes responsible for electromagnetic excitation of nuclei is commonly described as follows. When a nucleus absorbs one or two virtual photons with energy ω in the GDR region, $6 \le \omega \le 30$ MeV, the nucleus is supposed to be in a two particle, one hole (2p-1 h), exciton configuration as customarily adopted in the theory of preequilibrium reactions [40]. Preequilibrium emission of protons and neutrons is possible: it is particularly relevant for light nuclei where the GDR cross section peaks at higher energies. After thermalization, the nuclear deexcitation proceeds through evaporation, fission, or, for light nuclei, Fermi breakup and it is completely determined by the residual nucleus A, Z, and excitation energy $E^\star$. Since a lead nucleus has a high fission threshold, its GDR de-excitation proceeds mainly through the evaporation of neutrons with separation energies only around 7–8 MeV. Because of a high Coulomb barrier, proton emission is less relevant but still possible in the GDR region. The quasideuteron process, $\gamma + (np) \to n + p$, becomes important at $\omega \ge 40$ MeV and makes possible the emission of protons along with neutrons. Above the single-pion production threshold at $\omega = 140$ MeV the photoabsorption on a single nucleon is possible via the $\gamma N \to \pi N$ reaction, mainly by Δ resonance excitation. Finally, multiple pion production comes into play above the Δ-resonance region.

The excitation energy $E^\star$ transferred to a nucleus by virtual photons is much lower on average than that transferred in hadronic reactions. Therefore, the proton preequilibrium emission and evaporation channels are the main contributors to the mechanism changing the projectile charge state in ultraperipheral collisions. In the following we investigate single electromagnetic dissociation process where dissociation takes place *at least* for one of the nuclei in beam-beam collisions. Mutual electromagnetic dissociation cross section for reactions on a fixed target is known

to be small compared to the total cross section of the single EMD [41]. Its contribution of about 1% is well below the experimental errors and smaller than theoretical uncertainties in the treatment of the single EMD. Therefore, only single electromagnetic dissociation is considered in the present study.

In simulating EMD the FLUKA model starts from elementary photon-nucleon and photon-nucleus cross sections internally computed. It includes four different regimes for the photon-nucleus interactions: GDR, quasideuteron, resonance (mostly Delta), and high energy described through the vector meson dominance model.

According to this concept, all known physical processes responsible for electromagnetic excitation of nuclei beginning from the threshold of the photoneutron production reaction in the GDR region up to the LHC energies are considered to contribute to $\sigma_\gamma(\omega)$. The photonuclear cross sections in the GDR region have been evaluated from experimental data whenever possible, and are stored in a database isotope by isotope. For the other processes they are internally computed.

Such an approach can render the simulation procedure very time consuming if one employs numerical integration which folds together the appropriate equivalent photon spectrum $n(\omega)$ and the cross sections $\sigma_\gamma(\omega)$. This is particularly true of the GDR region, the most important one for EMD, where cross sections can exhibit significant structure. To avoid this problem, an analytical integration procedure has been developed for the EMD implementation into the FLUKA models. For each target isotope, the photon energy range is divided into several intervals, and the behavior of $\sigma_\gamma(\omega)$ is approximated with Bezier curves, which in turn allow for an analytical integration of the folding integral. It should be emphasized that this algorithm allows fast automatic fit of the input data and thus fast upgrade of the cross section database for hundreds of nuclides. The fit is performed without increasing the uncertainty of the measured photonuclear cross sections. Specifically, systematic uncertainties introduced by the fit are substantially lower than typical discrepancies between data on photonuclear reactions from different groups.

Once an electromagnetic dissociation event is selected, the model samples the virtual photon energy and minimum photon virtuality q^2 which is kinematically allowed. The equivalent real photon energy E_γ which would correspond to the same nuclear excitation is used for evaluating the cross section. The final state is generated taking fully into account the virtuality of the photon, so that energy and momentum conservation are fulfilled exactly.

B. Electromagnetic dissociation of nonrelativistic heavy ions

Cosmic rays provide a rich source of high energy ions bombarding spaceships and space probes. A substantial fraction of cosmic ray spectra is in the intermediate energy range with typical Lorentz γ factors ~1.1–2.0. At nonrelativistic energies Coulomb excitation can also be expressed in terms of equivalent photon numbers. Contrary to the relativistic case, in this event the field of quasireal photons contains all multipolarities with the same weight. The photonuclear cross section is then a sum of the contributions from all multipolarities, although only a few contribute in most processes [42].

A detailed comparison between relativistic and nonrelativistic calculations of the equivalent photon spectra for the electromagnetic interaction of intermediate-energy nuclei has been performed in Ref. [43]. The approach involves a semiclassical calculation with relativistically corrected trajectories in peripheral collisions which included both electric and magnetic excitations (multipoles) and their dependence on the impact parameter b. It has been shown that at the projectile energies of $\sim 0.1A$ GeV neither nonrelativistic nor relativistic approach could reproduce correct values of the cross section evaluated by taking into account both relativistic and nonrelativistic effects. The approach [43] yields the partial photonuclear absorption cross sections $\sigma_\gamma^{\pi\lambda}$ for a given multipolarity $\pi\lambda$. The total photonuclear cross section is well approximated by a sum of multipolarities $\pi\lambda$ giving the largest contribution at a given projectile energy E_0:

$$\sigma_{\mathrm{tot}}^{\gamma A}(E_0) = \sum_{\pi\lambda} \sigma_{\pi\lambda}^{\gamma}(E_0), \tag{6}$$

$$\sigma_{\pi\lambda}^{\gamma}(E_0) = \int_{\omega_{\mathrm{th}}}^{\omega_{\mathrm{max}}} \frac{d\omega}{\omega} n_{\pi\lambda}(E_0,\omega)\sigma_{\pi\lambda}^{\gamma}(\omega). \tag{7}$$

In relativistic collisions, the number of equivalent photons $n_{\pi\lambda}(E_0,\omega,b)$ per unit area $\mathrm{d}^2b = 2\pi b\mathrm{d}b$ involving three dominant multipolarities E1, E2 and M1 is given by

$$\frac{\mathrm{d}n_{E1}}{2\pi b\mathrm{d}b} = \frac{Z_2^2\alpha}{\pi^2}\frac{\xi^2}{b^2}\left(\frac{c}{v}\right)^2\left(K_1^2 + \frac{1}{\gamma^2}K_0^2\right), \tag{8}$$

$$\frac{\mathrm{d}n_{E2}}{2\pi b\mathrm{d}b} = \frac{Z_2^2\alpha}{\pi^2 b^2}\left(\frac{c}{v}\right)^4 \times \left[\frac{4}{\gamma^2}(K_1^2 + \xi K_0K_1 + \xi^2K_0^2) + \xi^2\left(2-\frac{v^2}{c^2}\right)^2K_1^2\right], \tag{9}$$

$$\frac{\mathrm{d}n_{M1}}{2\pi b\mathrm{d}b} = \frac{Z_2^2\alpha}{\pi^2}\frac{\xi^2}{b^2}K_1^2, \tag{10}$$

where K_0 and K_1 are the modified Bessel functions of the second kind of the argument $\xi(b) = \omega b/\gamma v$, and v is the ion velocity. These equations have been used in Ref. [43] for

TABLE I. Cross sections of electromagnetic dissociation of the ^{197}Au target with emission of one and two neutrons by low energy projectile ions.

Projectile Energy (GeV/n)	Beam ion	σ_{1n} (b) FLUKA	σ_{1n} (b) Experiment	σ_{2n} (b) FLUKA	σ_{2n} (b) Experiment	Experiment Reference
2.1	^{12}C	0.041	0.075 ± 0.014	0.009	0.009 ± 0.017	[45,49]
1.7	^{20}Ne	0.099	0.151 ± 0.013	0.020	⋯	[47]
2.1	^{20}Ne	0.102	0.153 ± 0.018	0.028	0.049 ± 0.014	[45,49]
1.8	^{40}Ar	0.303	0.348 ± 0.034	0.063	0.076 ± 0.018	[45,49]
1.7	^{56}Fe	0.595	0.601 ± 0.054	0.119	0.073 ± 0.013	[45,49]
1.0	^{86}Kr	0.851	0.820 ± 0.062	0.143	⋯	[47]
1.26	^{139}La	2.185	1.97 ± 0.13	0.388	0.335 ± 0.049	[49,50]
1.0	^{197}Au	3.528	3.077 ± 0.200	0.573	0.643 ± 0.105	[47]
9.89	^{197}Au	10.84	8.99 ± 0.53	2.65	2.32 ± 0.27	[51]
1.0	^{209}Bi	3.856	3.244 ± 0.205	0.627	⋯	[47]
0.96	^{238}U	4.454	3.16 ± 0.23	0.694	⋯	[46]

calculating equivalent photon numbers per unit area for the case of the Coulomb excitation induced by the ^{16}O nucleus incident with energy $0.1A$ GeV on a lead target. In this energy range, the virtual photon spectrum due to E2 transition [Eq. (9)] dominates over the M1 and E1 spectra. However, the cross section σ^{γ}_{E1} of the photoabsorption of E1 photons on nuclei in the region of GDR is the dominant one. This is why the consideration of the contribution from E1 virtual photons is a good approximation. The integration of Eq. (8) over the impact parameter by assuming the lower limit as $b_{\min} = R_1 + R_2$ yields [36]

$$n_{E_1}(\omega) = \frac{2Z_2^2\alpha}{\pi\omega}\xi^2\left(\frac{c}{v}\right)^2\left\{\frac{1}{\xi}K_0K_1 - \left(\frac{v}{c}\right)^2\frac{K_1^2 - K_0^2}{2}\right\}, \tag{11}$$

where $\xi = \omega(R_1 + R_2)/\gamma v$.

The expressions for the number of equivalent photons (8)–(11) can be used to describe photon spectra in intermediate (nonrelativistic) energy collisions if they are modified as suggested in Ref. [44]. It has been found that the photon spectra $n(E_0, \omega, b)$ of multipolarities M1, E1 and E2 evaluated in the nonrelativistic approach in a certain energy range, namely below $E_0 < 200A$ MeV, had the same shape as those obtained in relativistic calculations, and thus could be matched by the rescaling of the impact parameter in the following way:

$$b \to b + \frac{\pi a_0}{2\gamma}, \tag{12}$$

where a_0 is half the distance of the closest approach in a head-on collision in nonrelativistic kinematics defined as

$$a_0 = \frac{z_1 z_2 \alpha^2}{m_0 v^2}, \tag{13}$$

and

$$m_0 = \frac{m_1 m_2}{m_1 + m_2}. \tag{14}$$

The suggested approximation has been shown to yield photon spectra very close to those obtained by general expressions valid for all energies [43]. Namely, it has been found that at $E_0 \approx 0.5A$ GeV the relativistic approach with rescaling only slightly overestimates the photon number evaluated by the general expressions but the deviation reaches ~20% at $E_0 = 0.08A$ GeV, which can be considered as acceptable.

The quality of description of EMD processes in the region of low energies can be demonstrated by comparing calculations with experiments on one and two neutron separation performed with 1–2A GeV ions reported in Refs. [45,46]. The results of the comparison are shown in Table I. An overall agreement is good with the exception of a few cases in the $1n$ channel where the difference between the calculation and data is larger than 2 standard deviations. However, similar discrepancy between data and theoretical calculations based on WWA have been reported in Refs. [46–48]. The results in Table I indicate that the agreement with data from the $1n$ channel improves for ions starting from $A = 40$ but breaks down for the $0.96A$ GeV uranium beam. No reasonable explanation of the discrepancy in the latter case has been proposed [46].

IV. RESULTS OF CALCULATIONS AND COMPARISON TO EXPERIMENTAL DATA

A. Electromagnetic and nuclear cross sections for nucleus-nucleus collisions

Results of calculations for relativistic lead and gold ions can be confronted with available experimental data. We discuss first fragmentation of accelerated lead ions with Lorentz factors from $\gamma = 30$ to 2×10^7. This covers the range of energies from fixed target experiments at the CERN SPS to beam-beam collisions at the LHC collider. In the rest frame of one of the nuclei colliding at the LHC

projected energy of 7 TeV/charge per beam, the other nucleus is seen moving with the effective Lorentz factor $\gamma_{\text{eff}} = 1.7 \times 10^7$. This is the region in which the total and a few partial EMD cross sections by far exceed the total nuclear cross section of Pb-Pb interaction. The results of simulations obtained with FLUKA for the total EMD cross section, partial EMD cross sections corresponding to emission of one and two neutrons ($1nx$ and $2nx$, respectively), and for the total nuclear cross section are displayed in Fig. 1.

In Pb-Pb collisions at LHC energies, another process, the bound-free pair production [52] has a cross section comparable to that of EMD [5,53,54]; we do not discuss the calculation of that cross section here. Taken together, the sum of these cross sections determines the luminosity lifetime of the beam.

We compare the results of simulations with data on inclusive single and double neutron emission, $1nx$ and $2nx$ cross sections in electromagnetic dissociation of 30A GeV Pb nuclei on fixed targets available from Ref. [19], and with EMD and nuclear cross sections recently measured by ALICE collaboration at the energy $\sqrt{s_{\text{NN}}} = 2.76$ TeV [22]. The notations $1nx$ and $2nx$ are used to underline that the emission of undetected particles x other than neutrons is possible along with neutrons. In the energy range under consideration $1nx$ channel provides from 75% to 50% of the total EMD cross section, as predicted by the model, see Fig. 1. This is a consequence of the dominance of GDR excitation and its decay via $1n$ emission.

Although the $1nx$ channel is dominant, the contribution from $2nx$ emission is considered as an important feature of the model. Therefore, we have compared the results from FLUKA with available data for the ratio of EMD cross sections corresponding to the emission of two and one neutrons in Fig. 2. The agreement with the data should be considered as reasonable. Further research is likely required for better understanding of the uncertainties of the ratio under study.

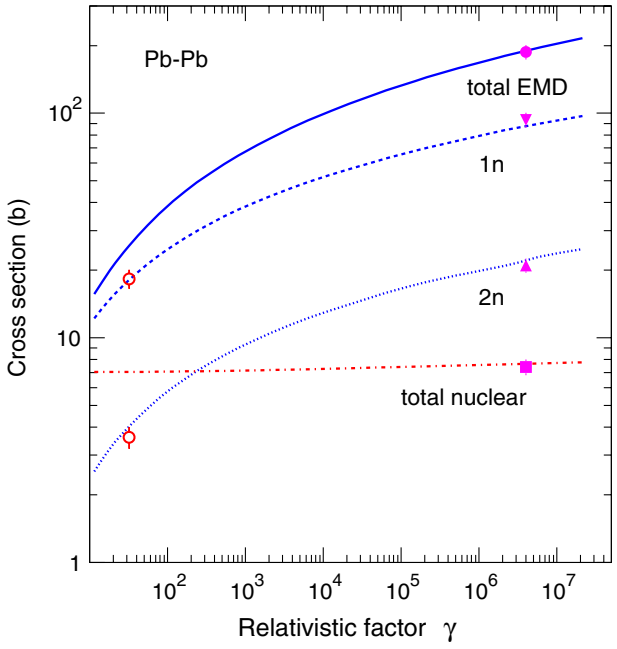

FIG. 1. Total electromagnetic dissociation and nuclear cross sections for Pb-Pb collisions as a function of the effective relativistic γ factor. The results of calculations of the total EMD cross section and partial cross sections in $1n$ and $2n$ channels are shown by solid, dashed and dotted lines, respectively. Total nuclear cross section calculated in the DPMJET-III model is shown by dot-dashed line. Results from the ALICE collaboration [22] for the total EMD and nuclear cross sections are shown by the full circle and full box, respectively. The measurements for $1n$ and $2n$ channels are shown by open circles [19] and full triangles [22].

B. Neutron emission cross sections

As found in Ref. [19], the measured $1nx$ and $2nx$ emission cross sections for 30A GeV Pb on Al, Cu, Sn and Pb reveal a quadratic dependence on target charge Z_t. In this experiment neutrons were measured in a very forward cone restricted by the transverse momentum $P_t = 0.15$ GeV/c. Neutrons produced in hadronic nucleus-nucleus collisions are expected to have a wider P_t distribution with average $\langle P_t \rangle \sim 0.2$–$0.4$ GeV/c. Therefore, one can suggest that the measured cross sections [19] can be considered as cross sections of EMD processes only. The data of Ref. [19] are plotted in Fig. 3 to be compared with FLUKA results for $1nx$ and $2nx$ channels of the EMD cross sections and with a sum of two channels.

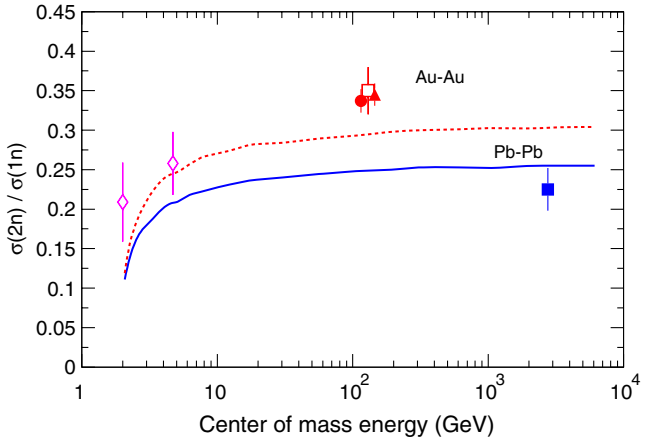

FIG. 2. Ratio of the electromagnetic dissociation cross sections in $2n$ and $1n$ channels as a function of the center of mass energy $\sqrt{s_{\text{NN}}}$ for the collisions of gold ions (upper curve) and lead ions (lower curve). Experimental data from the fixed target experiments [47,51] are shown with diamonds. The data from the RHIC experiments Phobos, Brahms and Phenix are displayed with the filled point, open square and filled triangle, respectively [55]. The filled square corresponds to the results from the ALICE [22] collaboration at the CERN LHC.

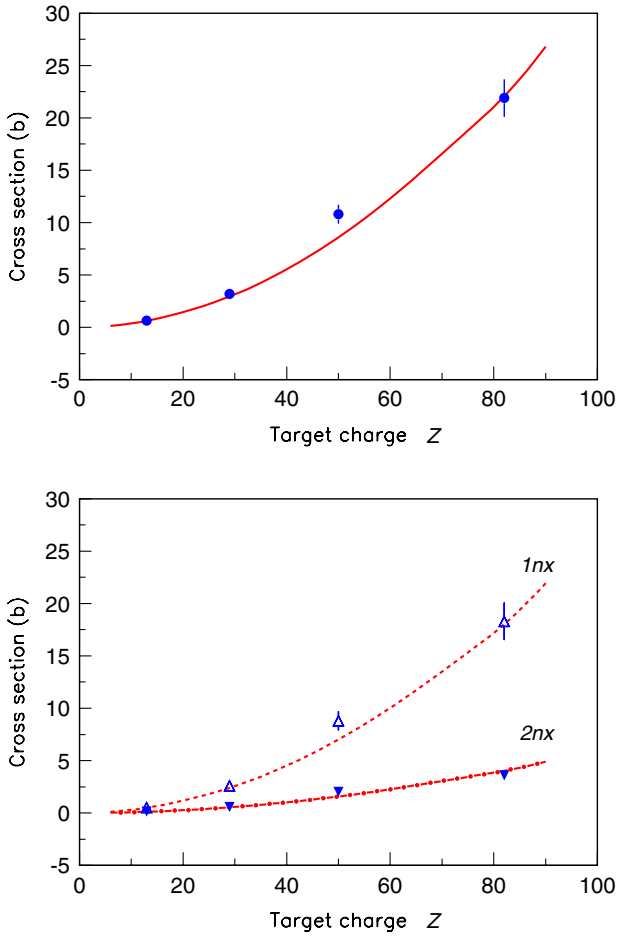

FIG. 3. (Top) Calculated (solid line) and measured (data points) sum of $1nx$ and $2nx$ electromagnetic dissociation cross sections as a function of the target charge. (Bottom) Calculated (dashed and dot-dashed lines) and measured (open and filled triangles) contributions from $1nx$ and $2nx$ channels, respectively, to the sum of $1nx$ and $2nx$ EMD cross sections. Data points are the measured cross sections of forward $1n$ and $2n$ emission in dissociation of 30A GeV Pb ions on Al, Cu, Sn and Pb targets [19].

We find a good agreement between FLUKA EMD results and experiment both for the sum of cross sections for $1nx$ and $2nx$ channels and for cross sections in each channel separately. Systematic uncertainties in the FLUKA simulation (not shown in Fig. 3) include systematic errors in experimental total photoneutron cross sections and theoretical errors of consideration of the reaction channels. Experimental errors are mainly due to inconsistencies in $1n$ and and $2n$ photoneutron cross sections measured in different laboratories. The problem has been discussed in Refs. [56,57] which include some prescriptions to rescale the original photoneutron data. We estimate ~25% as a typical calculational uncertainty for less prominent $2nx$, $3nx$ and higher multiplicity EMD channels.

C. Charge-changing heavy-ion interactions

The EMD reactions induced by the lead ions on medium and heavy nuclear targets have a significant probability to proceed with changing the projectile charge. The contribution of these events to the total cross section in Pb-Pb interaction at the LHC reaches about 50% according to the results at the largest values of γ displayed in Fig. 1. In what follows, we test the model under consideration by using data on charge-changing interactions of ions [16–18].

The total charge-changing cross section σ_{cc} is defined as the cross section of the process where the charge of the projectile nucleus Z_p changes because of charged particle emission. As a result, a fragment with charge Z_f is created, which in most cases corresponds to the negative charge difference $\Delta Z = Z_f - Z_p < 0$, mostly because of proton and heavier fragment emission. For the sake of completeness, EMD reactions with positive charge difference $\Delta Z > 0$ proceeding through π^- photoproduction, $\gamma n \to p\pi^-$, followed by pion escape, should be mentioned, see Ref. [58] for details. The contribution of the reactions with $\Delta Z > 0$ to σ_{cc} is very small compared to that with $\Delta Z < 0$.

Charge-changing reactions were studied in an experiment performed with 158A GeV Pb ions at the CERN SPS as reported in Refs. [16,58]. The data for σ_{cc} are plotted in Fig. 4 as a function of target mass A_t along with FLUKA results. Nuclear and electromagnetic contributions to σ_{cc} were not separated in the experiment and the models can only be tested

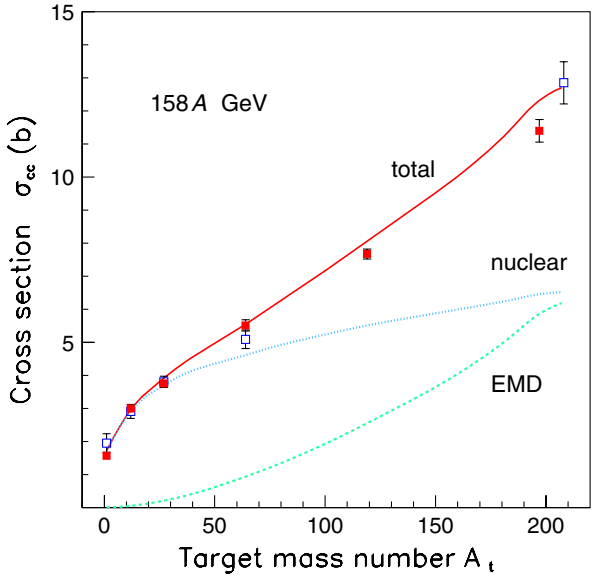

FIG. 4. Total charge-changing cross sections for the incident 158A GeV Pb ions as a function of target mass number. Electromagnetic contributions calculated by FLUKA are shown by the dashed line. The nuclear contributions calculated in the framework of DPMJET-III are shown by a dotted line and the sum of EMD and nuclear cross sections is displayed with the solid line. The data of Ref. [16] and Refs. [17,18] are shown by the full and open squares, respectively.

through the sum of such contributions, as shown in Fig. 4. The reaction cross section σ_{cc} for all target nuclei is fairly well described by the sum of nuclear and electromagnetic contributions evaluated with FLUKA simulation tools. To a reasonably good approximation, σ_{cc} can be calculated as the difference between the total reaction cross section and the cross section for fragmentation with only neutron emission:

$$\sigma_{cc} = \left(\sigma^{\mathrm{nuc}} - \sum_A \sigma^{\mathrm{nuc}}(Z=82)\right) + \left(\sigma^{\mathrm{EMD}} - \sum_A \sigma^{\mathrm{EMD}}(Z=82)\right). \quad (15)$$

Here the reaction cross section σ^{nuc} is evaluated in the framework of the embedded Glauber calculus for FLUKA with DPMJET-III. The models responsible for evaporation, fission, and fragmentation are the same upgraded versions used in PEANUT of those described in Refs. [23,30,31]. Those models are used both in the PEANUT and DPMJET-III event generators in order to describe the deexcitation of excited nuclear fragments left over from the fast stages of the nucleus-nucleus or (virtual) photon-nucleus interactions.

The hadronic contribution to σ_{cc} is obtained by subtracting a small part, about (0.47–0.63) b, of mostly peripheral reactions that do not change the charge state ($\Delta Z = 0$) from the total hadronic cross section of ~(2.0–7.4) b, depending on the target mass. On the contrary, the ($\Delta Z = 0$) reactions constitute a *major* part (~85%–90%) of the total EMD cross sections at 158*A* GeV. This is explained by the dominant contribution of GDR excitation followed by subsequent neutron emission.

We observe good agreement between the simulation with FLUKA and the data obtained on H, C, Al, Cu and Pb targets. FLUKA somewhat overestimates σ_{cc} for Sn and Au targets.

A detailed comparison between data on charge-changing interactions of 158*A* GeV ^{208}Pb projectiles with nuclear targets and calculations in the framework of FLUKA model is given in Fig. 5. There, the cross sections $\sigma(Z)$ of the production of nuclear fragments in the charge state Z are shown. Cross sections of the production of heavy fragments are displayed in zoom mode in Fig. 6. Additionally, data obtained in the charge pickup reactions are shown for $Z = 83$. In all cases a fair agreement between FLUKA simulation and experiments is observed demonstrating once again the importance of EMD processes on heavy targets and for heavy projectiles.

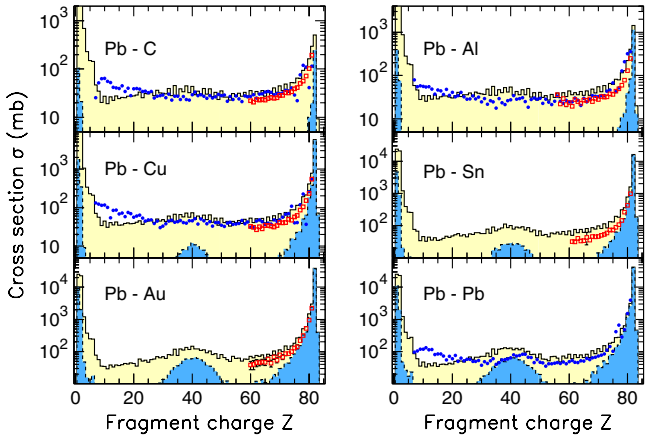

FIG. 5. Inclusive cross sections for producing a fragment with charge Z by 158*A* GeV ^{208}Pb projectiles on C, Al, Cu, Sn, Au and Pb targets. Experimental data from Ref. [16] and Refs. [17,18] are shown by the open squares and full circles, respectively. Results of the FLUKA model for electromagnetic dissociation are shown by the dashed (blue) histograms. The solid (yellow) histograms represent the sum of electromagnetic and hadronic contributions with the latter calculated in the DPMJET-III model.

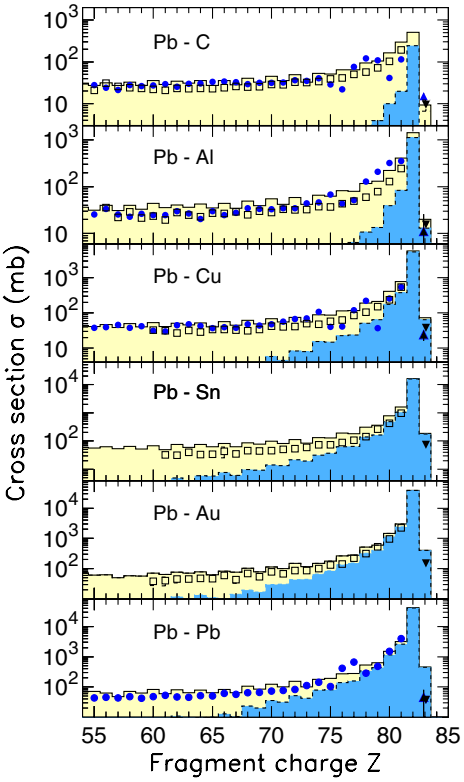

FIG. 6. Inclusive cross sections for producing a fragment with charge Z by 158*A* GeV ^{208}Pb projectiles on C, Al, Cu, Sn, Au and Pb targets. Experimental data from Refs. [16] and [17] are shown by the open squares and full circles, respectively. Charge pickup cross sections are shown by downward [16] and upward [18] triangles, respectively. The results for electromagnetic dissociation are shown by the dashed (blue) histograms. The solid (yellow) histograms represent the sum of electromagnetic and hadronic contributions evaluated in the framework of the FLUKA model.

V. HEAVY-ION FRAGMENTATION AT THE LHC

A. Interaction of the LHC beam with various materials

The total cross sections for electromagnetic dissociation and hadronic fragmentation of ^{208}Pb ions on fixed targets at the LHC injection energy of 177.4A GeV and the energy of 106.4A GeV which is used in the studies of collimation hardware at the CERN SPS [20] are given in Table II. The eleven target nuclei which were chosen for calculations include elements composing residual beam pipe gas—^{4}He, ^{12}C, ^{14}N and ^{16}O, solid-state materials from accelerator environment—^{9}Be, ^{27}Al, ^{56}Fe, ^{64}Cu, ^{184}W, the material used for production of bent crystals, ^{28}Si, proposed for crystal-assisted collimation [59], and ^{208}Pb. Hadronic nuclear fragmentation dominates in Pb interaction with the residual gas nuclei. The sum of σ^{EMD} and σ^{nuc} is also given for each target nucleus.

The total cross sections for electromagnetic dissociation and hadronic fragmentation of ^{208}Pb ions on fixed targets at the LHC collision energies of 1.58 and 2.75A TeV which correspond to the LHC beam energy 3.5 TeV per charge in the years 2010–2011 and to the full LHC energy of 7 TeV per charge, respectively, are given in Table III. As is apparent from the latter table, the electromagnetic contribution to the beam fragmentation becomes important for nuclei heavier than Al, and cannot be neglected in the total cross section. Moreover, it becomes dominant on fixed W and Pb targets which makes it a factor 10 larger than σ^{nuc} even at the first stage of the LHC ion beam energy of 1.58A TeV. The evaluated cross sections can be used to estimate the total interaction probability of lead ions with various materials at full LHC energy of 2.75A TeV. The influence of atomic screening has been neglected in these calculations. If taken into account, the total cross sections are expected to decrease by 7% and 12% for copper and tungsten targets (once considered as optional materials for the LHC collimation), respectively [60,61], at full LHC energy. The decrease is about the same order as estimated uncertainty in the total cross section. Moreover, this trend does not result in the underestimation of potential damage to the LHC equipment.

The experimental total charge-changing cross section σ_{cc} ($\Delta Z < 0$) of 158A GeV ions on H, C, Al, Cu, Sn, Au and Pb nuclei are evaluated in the FLUKA model within an uncertainty of about 5%. According to the results obtained in [16], in nucleus-nucleus hadronic interactions at high energies, the contribution of $\Delta Z = 0$ channels with emission of neutrons alone is very small compared to σ_{cc} cross section. Therefore, the total charge-changing cross section serves as a very good approximation to σ^{nuc}. At least for reactions on H, He, Be, C, N, O, and Al target nuclei, where nuclear contribution dominates, one can claim a similar 5% uncertainty for σ^{nuc}. Since nuclear and electromagnetic contributions to σ_{cc} are comparable for heavy targets, it is less straightforward to estimate separately the uncertainty of calculations for each contribution.

At the LHC energies, the sum of $1n$ and $2n$ channels in electromagnetic dissociation of lead nuclei is more than 50 percent of σ^{EMD}. According to the results obtained in Sec. IV B, the EMD cross section at lower energies for the nuclei under consideration is well described as a sum of $1n$ and $2n$ channels. Therefore, one can estimate an uncertainty of about 5% for σ^{EMD} at the energies of the LHC collider.

The cross sections listed in Table III are visualized in Fig. 7. We estimate the contribution of the cross sections for electromagnetic dissociation on target electrons to the total cross section to be of the order of ~1–2% which is well within calculation uncertainties of σ^{EMD} and σ^{nuc} and can

TABLE II. Total electromagnetic and hadronic fixed target cross sections and their sum in units of barn for interaction of 177.4 and 106.4A GeV/c Pb ions with nuclei composing materials from beam environment.

	σ (b), $p = 177.4A$ GeV/c			σ (b), $p = 106.4A$ GeV/c		
Target	EMD	Nuclear	Total	EMD	Nuclear	Total
He	0.035	2.53	2.56	0.031	2.52	2.55
Be	0.135	3.09	3.22	0.118	3.08	3.20
C	0.290	3.18	3.47	0.270	3.17	3.44
N	0.406	3.28	3.69	0.361	3.27	3.63
O	0.524	3.44	3.96	0.470	3.43	3.90
Al	1.34	4.02	5.36	1.18	4.01	5.19
Si-28	1.64	4.06	5.70	1.39	4.05	5.44
Fe	5.20	4.85	10.05	4.58	4.84	9.42
Cu	6.62	5.01	11.63	5.68	5.00	10.68
W	40.0	6.83	46.8	35.38	6.82	42.2
Pb-208	48.5	7.07	55.6	42.18	7.06	49.2

TABLE III. Total electromagnetic and nuclear fixed target cross sections in units of barn for interaction of 1.58 and 2.75A TeV/c Pb ions with nuclei composing materials from the beam environment.

	σ (b), $p = 1.58A$ TeV/c		σ (b), $p = 2.75A$ TeV/c	
Target	EMD	Nuclear	EMD	Nuclear
He	0.052	2.58	0.058	2.60
Be	0.202	3.12	0.344	3.14
C	0.471	3.24	0.498	3.26
N	0.630	3.34	0.690	3.36
O	0.804	3.50	0.900	3.53
Al	2.13	4.09	2.21	4.11
Si-28	2.37	4.12	2.67	4.15
Fe	8.27	4.92	9.02	4.94
Cu	10.16	5.09	11.05	5.11
W	63.52	6.92	68.91	6.95
Pb-208	77.87	7.16	84.61	7.19

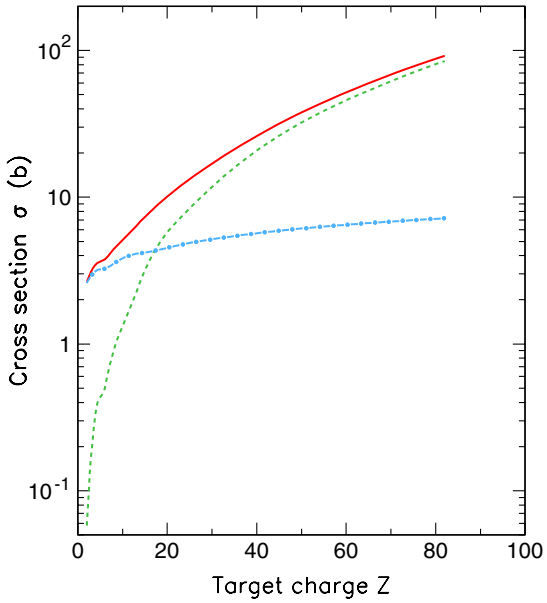

FIG. 7. Total (solid line), electromagnetic dissociation (dashed line) and nuclear fragmentation (dot-dashed line) cross sections for the incident lead ions on target nuclei as a function of the nuclear charge Z evaluated for the projected LHC energy of 7 TeV/charge.

thus be neglected in further studies. Moreover, this EMD reaction does not occur in collisions of fully stripped beam ions.

B. Beam-beam interaction at the LHC

The total cross sections for the reactions induced by beam-beam collisions at the LHC are listed in Tables IV and V for collision energies of 1.38A TeV and 2.75A TeV, respectively, separately for electromagnetic dissociation and nuclear interactions. The results shown in Table IV are in a good agreement with both calculations based on the RELDIS model and recent LHC data reported by the ALICE Collaboration [22]. The cross sections σ^{EMD} from Refs. [7,11,62] listed in Table V are in a good agreement with the result obtained within the approach under discussion.

We estimate the uncertainty of the integration procedure in calculating σ^{EMD} via a convolution of the total photonuclear cross section and equivalent photon spectrum at the level of ~5%. The dominant contribution to the latter number is due to experimental uncertainties in total photonuclear cross sections [63]. Also, one notes that the results of four different calculations of σ^{EMD} shown in Table V are in agreement within 3%.

TABLE V. Total electromagnetic and nuclear cross sections (barn) for colliding lead ion beams at 2.75 + 2.75A TeV.

Reaction	FLUKA	RELDIS [11]	Ref. [7]	Ref. [62]
Single EMD + nuclear	219.8	222.9	...	...
Nuclear	7.81	7.88	...	...
Single EMD	212	215	214	220

C. Mass, charge and momentum distributions of the fragments produced in peripheral collisions of LHC lead ions

Nuclear fragmentation and electromagnetic dissociation of ions which occur in the LHC collimation system produce fragments close in mass and charge to beam ions. The fragments have similar magnetic rigidity and, therefore, remain close to the beam trajectory in the LHC ring for a long distance from the interaction point. This is primarily true for fragments created in electromagnetic dissociation of beam ions. It is a purpose of the LHC collimation system to remove such fragments prior to unwanted interactions with accelerator components.

We have simulated the mass, charge and momentum distributions of beam fragments. The excitation of the giant dipole resonance in a lead nucleus dominates the electromagnetic dissociation induced by soft photons. The GDR decay process is followed mostly by neutron evaporation, resulting in a single heavy residual nucleus. Photonuclear reactions induced by more energetic virtual photons on a Pb nucleus occur with lower probability and the emission of a single heavy nucleus dominates in the exit channel after knock-out of intranuclear nucleons or meson photoproduction. Additionally, other less frequent reactions may occur producing light nuclear fragments—^{2}H, ^{3}H, ^{3}He, ^{4}He and others. The latter, as corroborated by the simulation, have a considerable probability to stay in the LHC ion beam and, therefore, have to be taken into account in the studies involving ion beam passage. Furthermore, EMD reactions induced by beam-beam interactions at the LHC may

TABLE IV. Total electromagnetic and nuclear cross sections (barn) for Pb-Pb interactions at the energy $\sqrt{s_{\mathrm{NN}}} = 2.76$ TeV.

Reaction	FLUKA	RELDIS [22]	ALICE experiment [22]
Single EMD + nuclear	197.7	192.9 ± 9.2	$194.8 \pm 0.3\,\mathrm{stat} + 13.6/-11.5\,\mathrm{syst}$
Nuclear	7.67	7.7 ± 0.4	$7.7 \pm 0.1\,\mathrm{stat} + 0.6/-0.5\,\mathrm{syst}$
Single EMD	190.	185.2 ± 9.2	$187.4 \pm 0.2\,\mathrm{stat} + 13.2/-11.2\,\mathrm{syst}$

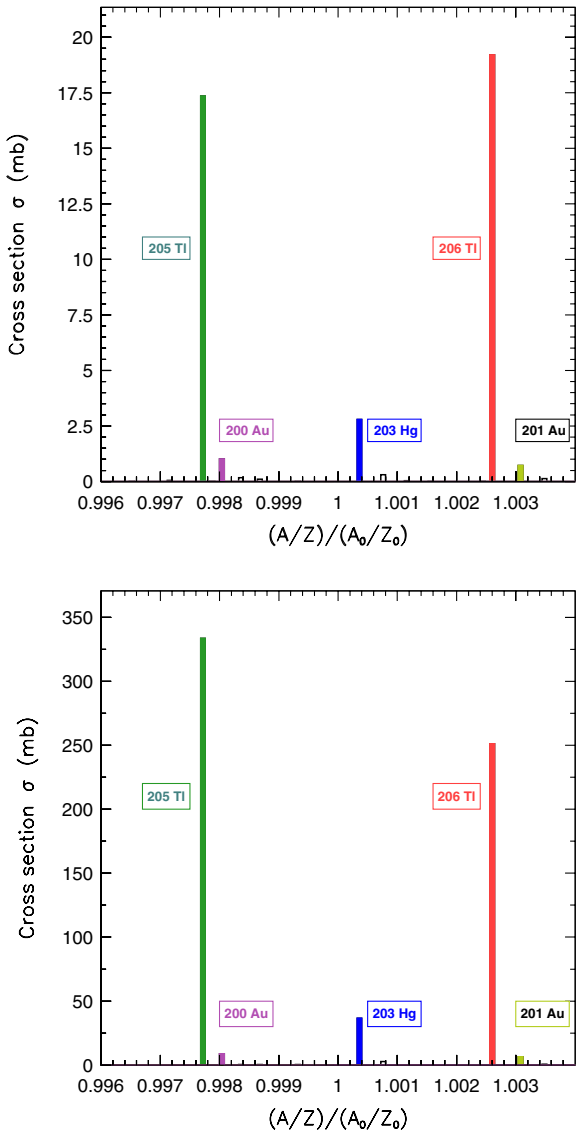

FIG. 8. Cross sections for the production of the heaviest fragments in electromagnetic dissociation of 2750A GeV Pb nuclei on ^{12}C (top panel) and ^{74}W (bottom panel) targets as a function of the mass-to-charge ratio normalized to that of the main circulating beam. A contribution from nuclear fragments other than indicated by filled bars is shown with unfilled bars.

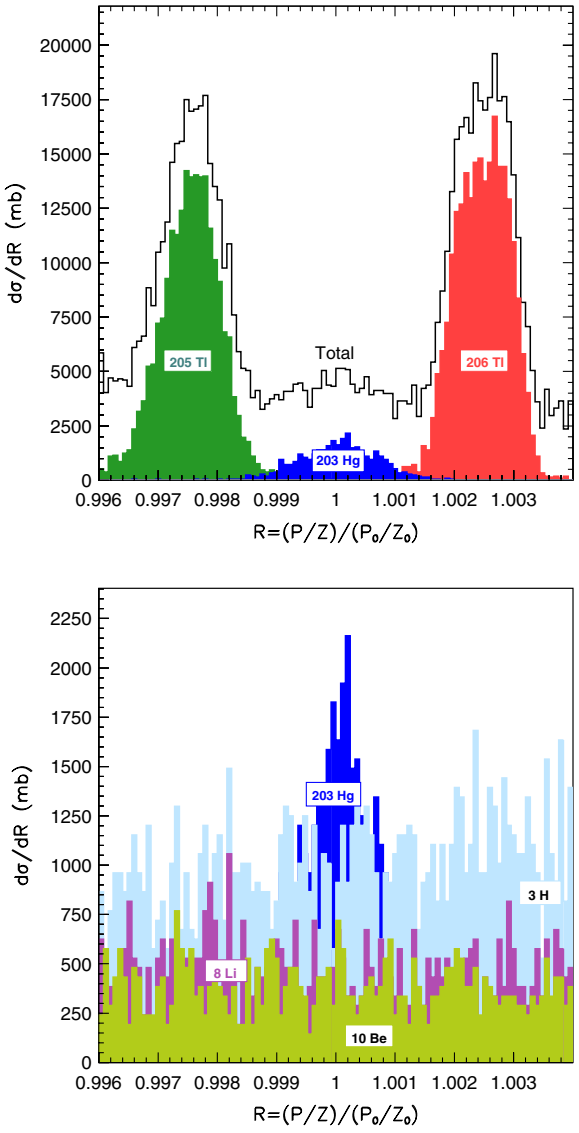

FIG. 9. Cross sections for the production of the heaviest (top panel) and light (bottom panel) fragments (together with ^{203}Hg) in electromagnetic dissociation of 2750A GeV Pb nuclei on ^{12}C target as a function of the momentum-to-charge ratio normalized to that of the main circulating beam.

involve more complex configurations including nuclear fission.

Each simulation run of FLUKA involved 10^6 electromagnetic dissociation events produced in kinematic conditions corresponding to the LHC lead ion beam interaction with graphite used for the collimator jaws and tungsten. As it is found from simulation, nearly 50% of ions have magnetic rigidity differing by less than 0.5% from that of initial ^{208}Pb ions. The cross sections for production of fragments as a function of a normalized mass-to-charge ratio are shown in Fig. 8. In addition to small changes of the rigidity A/Z for the produced fragments, the simulations demonstrate a decrease of the order of 1 GeV/c in the fragment longitudinal momentum caused by stopping due to absorption of virtual photons involved in EMD reactions. Even if the typical recoil momentum of the fragment is below 100 MeV/c in the rest frame of the circulating lead ion beam the Lorentz boost to the laboratory frame changes the fragment momentum by a value up to a few GeV/c. As a result, the simulations demonstrate characteristic Gaussian-like distributions for the fragment rigidity in terms of the momentum-to-charge ratio. Two examples representing the result of lead beam interactions on carbon and tungsten targets are displayed in Figs. 9 and 10, respectively. One

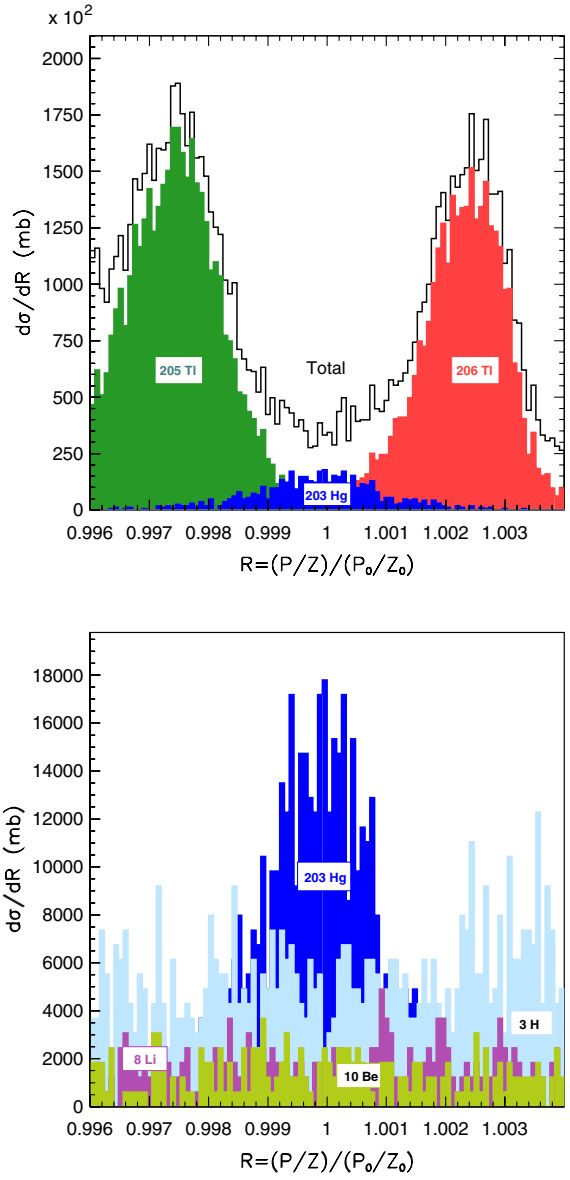

FIG. 10. Cross sections for the production of the heaviest (top panel) and light (bottom panel) fragments (together with ^{203}Hg) in electromagnetic dissociation of 2750A GeV Pb nuclei on ^{74}W target as a function of the momentum-to-charge ratio normalized to that of the main circulating beam.

finds that even light nuclear fragments, although with a low probability, can stay in the circulating beam by satisfying the condition $(P/Z)/(P_0/Z_0) = 1$, where P_0, Z_0 and P, Z denote the momentum and the charge of the main beam and those of nuclear fragments, respectively.

The longitudinal momentum P_l of the fragment produced in beam-beam collisions at the LHC can also be lower than that of the beam ion, whereas a small number of fragments stay in the circulating beam with a higher momentum. The latter can occur due to multiple particle photoproduction in which the recoil momentum of the

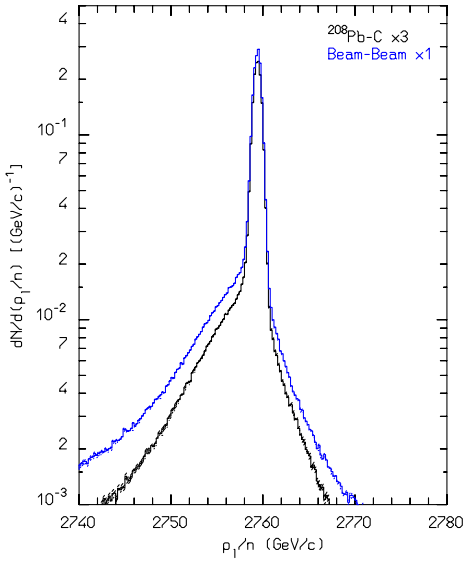

FIG. 11. Longitudinal momentum distribution for the heaviest fragment in electromagnetic dissociation of 2750A GeV ^{208}Pb ions interacting with stationary carbon nuclei (lower histogram), and in Pb-Pb beam collisions (upper histogram).

fragment is opposite to the direction of the photon. The resulting beam momentum profile is shown in Fig. 11.

The distribution of the heaviest fragment produced in the electromagnetic dissociation as a function of the transverse momentum P_t is shown in Fig. 12. The distribution reflects

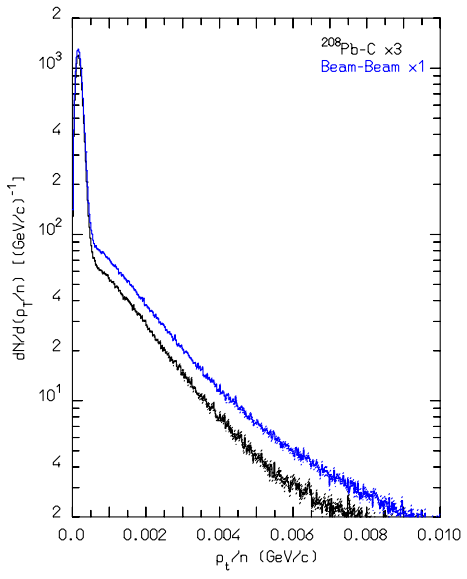

FIG. 12. Transverse momentum distribution for the heaviest fragment in electromagnetic dissociation of 2750A GeV ^{208}Pb ions interacting with stationary carbon nuclei (lower histogram), and in Pb-Pb beam collisions (upper histogram).

directly the P_t distribution of fragments in the rest frame of the initial nucleus. The main peak at low P_t originates from $1n$ and $2n$ emission events. However, larger P_t values correspond to reactions with more energetic photons above the GDR resonance leading to a long tail in P_t distribution seen in Fig. 12.

VI. CONCLUSIONS

We have developed a framework for fast and accurate simulation of hadronic fragmentation and electromagnetic dissociation of ultrarelativistic heavy ions that is now used as a basis for modeling heavy ion beam losses at the LHC collider at CERN. The simulation tools are based on a two-component dual parton model DPMJET-III, in the case of hadronic fragmentation and on the FLUKA EMD model in the event of electromagnetic dissociation of nuclei. Its validity has been verified by comparing results of the simulation with available data. Predictions of the yields of nuclear fragments close in mass and charge to initial beam ions are obtained.

The modeling of heavy-ion collimation processes in the LHC [4,20] has been realized without the simulation of EMD reactions described in the present paper. It proved to be quite successful in reproducing observed loss patterns in the SPS and LHC but is known to be incomplete in a number of respects. Among these, the selection of fragments emerging from the collimator jaws is incomplete (cuts on the mass and changes in rigidity are imposed so that very light fragments, for example, are ignored), transverse recoils are not completely modeled and the tracking through the accelerator optics is oversimplified. The tools provided here will allow some of these restrictions to be lifted and afford the potential to build more precise simulations that should lead to more accurate predictions.

More in general, the models described in this paper can be applied whenever the electromagnetic dissociation of nuclei at energies above a few hundreds of A MeV is of concern.

ACKNOWLEDGMENTS

We are grateful to R. W. Assmann, K. Schindl, and V. Vlachoudis for useful discussions and I. A. Pshenichnov for his contribution at the initial stage of this work. We also thank G. Bellodi, R. Bruce, and S. Gilardoni for their collaboration in developing applications to the SPS and LHC at various stages of this work. G. I. S. is grateful to the University of Houston for the support of his work. G. I. S. also acknowledges support from NASA Grants No. NAG8-1858 and No. NAG8-1901.

[1] H. Geissel, H. Weick, C. Scheidenberger, R. Bimbot, and D. Gardés, Nucl. Instrum. Methods Phys. Res., Sect. B **195**, 3 (2002).

[2] A. Voitkiv, Phys. Rep. **392**, 191 (2004).

[3] O. Brüning, P. Collier, P. Lebrun, S. Myers, R. Ostojic, J. Poole, and P. Proudlock (LHC Collaboration), Technical Report No. CERN/2004/003, 2004 [http://cds.cern.ch/record/782076].

[4] H. H. Braun, R. Assmann, A. Ferrari, J. B. Jeanneret, J. M. Jowett, and I. A. Pshenichnov, in *Proceedings of the 9th European Particle Accelerator Conference, Lucerne, 2004* (EPS-AG, Lucerne, 2004), p. 551.

[5] J. M. Jowett, H. H. Braun, M. I. Gresham, E. Mahner, A. N. Nicholson, I. A. Pshenichnov, and E. N. Shaposhnikova, in *Proceedings of the 9th European Particle Accelerator Conference, Lucerne, 2004* (Ref. [4]), p. 578.

[6] R. Bruce, J. M. Jowett, M. Blaskiewicz, and W. Fischer, Phys. Rev. ST Accel. Beams **13**, 091001 (2010).

[7] F. Krauss, M. Greiner, and G. Soff, Prog. Part. Nucl. Phys. **39**, 503 (1997).

[8] G. Baur, K. Hencken, D. Trautmann, S. Sadovsky, and Y. Kharlov, Phys. Rep. **364**, 359 (2002).

[9] A. J. Baltz, G. Baur, D. d'Enterria, L. Frankfurt, F. Gelis, V. Guzey, K. Hencken, Y. Kharlov, M. Klasen, S. Klein, Phys. Rep. **458**, 1 (2008).

[10] I. A. Pshenichnov, I. N. Mishustin, J. P. Bondorf, A. S. Botvina, and A. S. Iljinov, Phys. Rev. C **60**, 044901 (1999).

[11] I. A. Pshenichnov, J. P. Bondorf, I. N. Mishustin, A. Ventura, and S. Masetti, Phys. Rev. C **64**, 024903 (2001).

[12] I. A. Pshenichnov, Phys. Part. Nucl. **42**, 215 (2011).

[13] A. Ferrari, P. R. Sala, A. Fassò, and J. Ranft, Reports No. CERN 2005-10, No. INFN/TC_05/11, and No. SLAC-R-773, 2005.

[14] G. Battistoni, S. Muraro, P. R. Sala, F. Cerutti, A. Ferrari, S. Roesler, A. Fassò, and J. Ranft, in AIP Conf. Proc. **896**, 31 (2007).

[15] S. Datz, J. R. Beene, P. Grafstrom, H. Knudsen, H. F. Krause, R. H. Schuch, and C. R. Vane, Phys. Rev. Lett. **79**, 3355 (1997).

[16] C. Scheidenberger, I. A. Pshenichnov, K. Sümmerer, A. Ventura, J. P. Bondorf, A. S. Botvina, I. N. Mishustin, D. Boutin, S. Datz, H. Geissel *et al.*, Phys. Rev. C **70**, 014902 (2004).

[17] S. Cecchini, G. Giacomelli, M. Giorgini, G. Mandrioli, L. Patrizii, V. Popa, P. Serra, G. Sirri, and M. Spurio, Nucl. Phys. **A707**, 513 (2002).

[18] H. Dekhissi, G. Giacomelli, M. Giorgini, G. Mandrioli, S. Manzoor, L. Patrizii, V. Popa, P. Serra, and V. Togo, Nucl. Phys. **A662**, 207 (2000).

[19] M. B. Golubeva, F. F. Guber, T. L. Karavicheva, E. V. Karpechev, A. B. Kurepin, A. I. Maevskaya, I. A. Pshenichnov, A. I. Reshetin, K. A. Shileev, V. V. Tiflov *et al.*, Phys. Rev. C **71**, 024905 (2005).

[20] R. Bruce, R. W. Assmann, G. Bellodi, C. Bracco, H. H. Braun, S. Gilardoni, E. B. Holzer, J. M. Jowett, S. Redaelli, and T. Weiler, Phys. Rev. ST Accel. Beams **12**, 011001 (2009).

[21] C. Oppedisano *et al.* (ALICE Collaboration), J. Phys. G **38**, 124174 (2011).

[22] B. Abelev, J. Adam, D. Adamová, A. M. Adare, M. M. Aggarwal, G. A. Rinella, A. G. Agocs, A. Agostinelli, S. A. Salazar, Z. Ahammed *et al.* (ALICE Collaboration), Phys. Rev. Lett. **109**, 252302 (2012).

[23] A. Ferrari and P. R. Sala, in *Proceedings of the Workshop on Nuclear Reaction Data and Nuclear Reactors Physics, Design and Safety, International Center for Theoretical Physics, Miramare-Trieste, Italy, 1996*, edited by A. Gandini and G. Reffo (World Scientific, Singapore, 1998), Vol. **2**, pp. 424–532 [http://inspirehep.net/record/1195022?ln=en].

[24] A. Fassò, A. Ferrari, J. Ranft, and P. R. Sala, in *Proceedings of the Monte Carlo 2000 Conference, Lisbon*, edited by A. Kling, F. Barão, M. Nakagawaand, L. Távora, and P. Vaz (Springer-Verlag Berlin, 2001), pp. 955–960.

[25] G. Battistoni, F. Cerutti, R. Engel, A. Fassò, A. Ferrari, E. Gadioli, M. V. Garzelli, J. Ranft, S. Roesler, and P. R. Sala, in *Proceedings of the 11th International Conference on Nuclear Reaction Mechanisms, Varenna, Italy, 2006*, edited by E. Gadioli (University of Milano, 2006).

[26] F. Ballarini, G. Battistoni, F. Cerutti, A. Empl, A. Fassò, A. Ferrari, E. Gadioli, M. V. Garzelli, A. Ottolenghi, L. S. Pinsky, J. Ranft, S. Roesler, P. R. Sala, and G. Smirnov, in *Proceedings of the International Conference on Nuclear Data for Science and Technology, Santa Fe, NM*, AIP Conf. Proc. No. 769 (AIP, New York, 2005), pp. 1197–1202.

[27] F. Ballarini *et al.* (FLUKA Collaboration), Adv. Space Res. **40**, 1339 (2007).

[28] F. Cerutti, A. Ferrari, A. Mairani, and P. R. Sala, in *Proceedings of the 13th International Conference on Nuclear Reaction Mechanisms, Varenna, Italy* (2012), pp. 469–475 [http://cdsweb.cern.ch/record/1495183].

[29] T. Boehlen, F. Cerutti, M. Chin, A. Fassò, A. Ferrari, P. Ortega, A. Mairani, P. Sala, G. Smirnov, and V. Vlachoudis, in *Proceedings of the International Conference on Nuclear Data for Science and Technology, New York, NY, 2013 [Nuclear Data Sheets (to be published)].*

[30] A. Ferrari, P. R. Sala, J. Ranft, and S. Roesler, Z. Phys. C **70**, 413 (1996).

[31] A. Ferrari, J. Ranft, S. Roesler, and P. R. Sala, Z. Phys. C **71**, 75 (1996).

[32] J. Ranft, Phys. Rev. D **51**, 64 (1995).

[33] S. Roesler, R. Engel, and J. Ranft, arXiv:hep-ph/0012252.

[34] H. Sorge, H. Stöcker, and W. Greiner, Ann. Phys. (N.Y.) **192**, 266 (1989).

[35] V. Andersen, F. Ballarini, G. Battistoni, M. Campanella, M. Carboni, F. Cerutti, A. Empl, A. Fasso, A. Ferrari, E. Gadioli *et al.*, Adv. Space Res. **34**, 1302 (2004).

[36] D. Jackson, *Classical Electrodynamics* (Wiley, New York, 1999).

[37] G. Baur, K. Hencken, and D. Trautmann, J. Phys. G **24**, 1657 (1998).

[38] A. Fassò, A. Ferrari, and P. R. Sala, in *Proceedings of the 8th International Conference Radiation Shielding, Arlington, Texas, 1994* (American Nuclear Society, Arlington, TX, 1994), Vol. **2**, p. 643.

[39] A. Ferrari and P. R. Sala, Radiation Protection Dosimetry **99**, 29 (2002).

[40] M. B. Chadwick and P. G. Young, *Acta Phys. Slovaca* **45**, 633 (1995).

[41] W. Llope and P. Braun-Munzinger, Phys. Rev. C **41**, 2644 (1990).

[42] C. A. Bertulani and G. Baur, Phys. Rep. **163**, 299 (1988).

[43] A. N. F. Aleixo and C. A. Bertulani, Nucl. Phys. **A505**, 448 (1989).

[44] A. Winther and K. Alder, Nucl. Phys. **A319**, 518 (1979).

[45] M. T. Mercier, J. C. Hill, F. K. Wohn, C. M. McCullough, M. E. Nieland, J. A. Winger, C. B. Howard, S. Renwick, D. K. Matheis, and A. R. Smith, Phys. Rev. C **33**, 1655 (1986).

[46] J. C. Hill, F. Wohn, D. Schwellenbach, and A. Smith, Phys. Lett. B **273**, 371 (1991).

[47] T. Aumann, J. V. Kratz, E. Stiel, K. Sümmerer, W. Brüchle, M. Schädel, G. Wirth, M. Fauerbach, and J. C. Hill, Phys. Rev. C **47**, 1728 (1993).

[48] J. C. Hill and F. K. Wohn, Phys. Rev. C **39**, 2474 (1989).

[49] J. C. Hill, F. K. Wohn, J. A. Winger, M. Khayat, M. T. Mercier, and A. R. Smith, Phys. Rev. C **39**, 524 (1989).

[50] J. C. Hill, F. K. Wohn, J. A. Winger, M. Khayat, K. Leininger, and A. R. Smith, Phys. Rev. C **38**, 1722 (1988).

[51] J. C. Hill, L. A. Ewell, B. Libby, F. K. Wohn, G. I. Crawford, W. J. Turner, J. B. Cumming, and C. J. Benesh, in Report No. WSU-NP-96-16, Wayne State University, 1996, pp. 286–290.

[52] The bound-free pair production can be considered as a Coulomb induced process occurring in $A_1 + A_2$ peripheral collisions in three steps: (1) the virtual photons generated by the Coulomb field of ultrarelativistic ion can create (2) e^+e^- pairs which yield electrons that can be captured (3) by a projectile: $\gamma + A \rightarrow e^+ + (Ae^-)$. A hydrogenlike atom is produced at the third step.

[53] A. J. Baltz, M. J. Rhoades-Brown, and J. Weneser, Phys. Rev. E **54**, 4233 (1996).

[54] R. Bruce, D. Bocian, S. Gilardoni, and J. M. Jowett, Phys. Rev. ST Accel. Beams **12**, 071002 (2009).

[55] M. Chiu, A. Denisov, E. Garcia, J. Katzy, A. Makeev, M. Murray, and S. White, Phys. Rev. Lett. **89**, 012302 (2002).

[56] E. Wolynec, A. R. V. Martinez, P. Gouffon, Y. Miyao, V. A. Serrão, and M. N. Martins, Phys. Rev. C **29**, 1137 (1984).

[57] B. L. Berman, R. E. Pywell, S. S. Dietrich, M. N. Thompson, K. G. McNeill, and J. W. Jury, Phys. Rev. C **36**, 1286 (1987).

[58] C. Scheidenberger, I. A. Pshenichnov, T. Aumann, S. Datz, K. Sümmerer, J. P. Bondorf, D. Boutin, H. Geissel, P. Grafström, H. Knudsen *et al.*, Phys. Rev. Lett. **88**, 042301 (2002).

[59] W. Scandale, G. Arduini, R. Assmann, C. Bracco, F. Cerutti, J. Christiansen, S. Gilardoni, E. Laface, R. Losito, A. Masi *et al.*, Phys. Lett. B **703**, 547 (2011).

[60] J. C. Baggesen and A. H. Sørensen, Nucl. Instrum. Methods Phys. Res., Sect. B **267**, 2662 (2009).

[61] Y. L. Pivovarov, *Izv. Vyssh. Uchebn. Zaved., Fiz.* **10/2**, 42 (2007).

[62] A. J. Baltz, C. Chasman, and S. N. White, Nucl. Instrum. Methods Phys. Res., Sect. A **417**, 1 (1998).

[63] For some nuclides this uncertainty can be even larger. The discussion of the problems in the measurements of photonuclear cross sections is beyond the scope of this paper.